AGU PUBLICATIONS

Geophysical Research Letters

RESEARCH LETTER
10.1002/2014GL062555

Special Section:
ESA's Swarm Mission, One Year in Space

Confirmation of existence of the small-scale field-aligned currents in middle and low latitudes and an estimate of time scale of their temporal variation

Toshihiko Iyemori[1], Kunihito Nakanishi[1], Tadashi Aoyama[1], Yoshihiro Yokoyama[1], Yukinobu Koyama[1], and Hermann Lühr[2]

[1]Graduate School of Science, Kyoto University, Kyoto, Japan, [2]Helmholtz-Centre Potsdam, GFZ German Research Centre for Geosciences, Potsdam, Germany

Key Points:
- Confirmation of existence of the small-scale FACs in midlatitude/low latitude
- Temporal scale of variation of the FACs is estimated by a new method
- Acoustic mode of gravity waves is suggested to be the source of FACs

Correspondence to:
T. Iyemori,
iyemori@kugi.kyoto-u.ac.jp

Citation:
Iyemori, T., K. Nakanishi, T. Aoyama, Y. Yokoyama, Y. Koyama, and H. Lühr (2015), Confirmation of existence of the small-scale field-aligned currents in middle and low latitudes and an estimate of time scale of their temporal variation, *Geophys. Res. Lett.*, *42*, 22–28, doi:10.1002/2014GL062555.

Received 18 NOV 2014
Accepted 16 DEC 2014
Accepted article online 19 DEC 2014
Published online 8 JAN 2015
Corrected 27 APR 2015

This article was corrected on 27 APR 2015. See the end of the full text for details.

Abstract The magnetic data obtained by the SWARM (the Earth's Magnetic Field and Environment Explorers) satellites in middle or low latitudes during the initial 2 months after launch were analyzed, when they flew nearly on the same orbit with variable time separation ranging from 5 to 100 s. It was confirmed that the small-scale magnetic fluctuations having period around 10–30 s are the manifestation of spatial structure of small-scale field-aligned currents along the orbits. From the statistical relation between correlation coefficients and two satellite separation in time, the typical time scale of temporal variation of the field-aligned current system is estimated to be around 200 s for meridional component and 340 s for zonal components of the magnetic fluctuations, respectively. Existence of shorter time scale around 30–50 s was also found. These results suggest that the main source of current generation is the acoustic mode of atmospheric gravity waves.

1. Introduction

Some electromagnetic effects in the ionosphere from lower atmosphere with time scale longer than several hours, such as geomagnetic lunar daily variation, are well known as a tidal effect. The phenomena with shorter time scale (i.e., from 10 min to several hours), such as medium-scale traveling ionospheric disturbance, are believed to be caused by the internal gravity waves although the source is not yet very clear. Most of the magnetic fluctuations with time scale shorter than 5 min observed on the ground are believed to come from the magnetosphere. Therefore, when we observe a wave-like magnetic fluctuations by satellite flying over middle or low-latitude ionosphere, we tend to interpret them as magnetic pulsations of magnetospheric origin. In particular, magnetic fluctuations having period around 20–40 s observed along the orbit by low-altitude satellites such as the CHAMP (altitude around 450–300 km) have been investigated as the Pc3 or Pc4 magnetic pulsations [e.g., *Heilig et al*., 2007, and references therein].

However, from an analysis of the magnetic field data obtained by the CHAMP satellite, it was found that the small spatial scale field-aligned currents exist in middle and low latitudes almost always [*Nakanishi et al*., 2014]. They concluded from their statistical characteristics that the small amplitude (a few nanotesla) magnetic fluctuations observed along the satellite orbit are essentially the spatial structure of the small spatial scale field-aligned currents rather than a temporal variation of geomagnetic field such as the Pc3 pulsations. That is, their results of analysis do not show any expected dependence on a geomagnetic activity index, *Kp*, on the latitude nor on the solar wind parameters having relation to known geomagnetic phenomena caused by space plasma processes. They showed a clear seasonal and geographical dependences which strongly suggest lower atmospheric origin such as atmospheric gravity waves. The tendency that the apparent period becomes longer as the satellite approaches to magnetic equator was also explained by the geometry of field-aligned currents and satellite orbit. However, these evidences are more or less indirect, and the time scale of their temporal variation, which is essential to identify the source mechanism, is unknown. *Nakanishi et al*. [2014] suggested that the temporal variation of the field-aligned currents is much slower than the time scale that the low-altitude satellite passes through a pair of field-aligned currents, i.e., 10–30 s (75–225 km in spatial scale). However, they could not examine the time scale from single satellite observation. In this paper, we confirm the existence of the

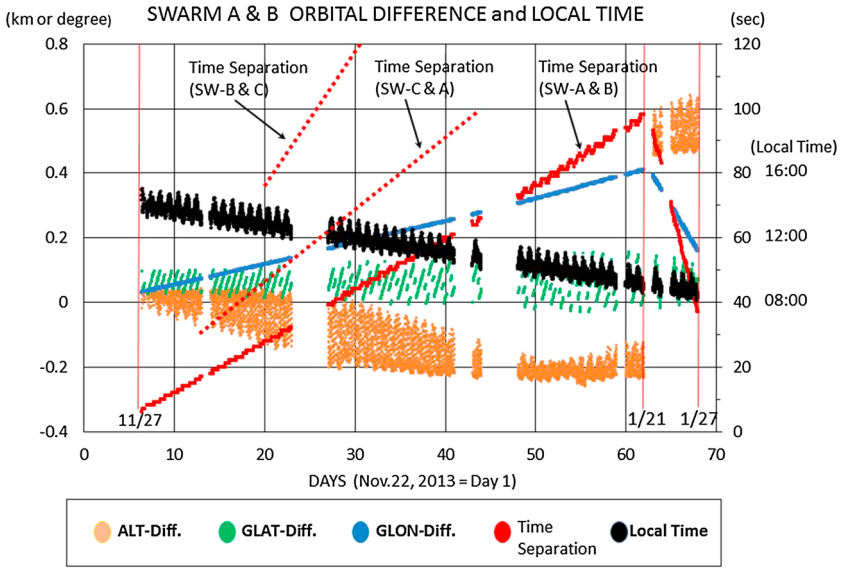

Figure 1. The separation of the time (in seconds; red dots) and of the geographical location (altitude (brown), latitude (green), and longitude (blue)) when the SWARM-A and SWARM-B pass the same geomagnetic (i.e., dipole) latitude. The local time (black) is also shown.

field-aligned currents more directly and propose an in-flight method to estimate the typical time scale of the temporal variation of the field-aligned currents from SWARM data analysis.

2. Data and Analysis

Until the end of January 2014 after the launch on 22 November 2013, the three satellites, SWARM-A, SWARM-B, and SWARM-C, flew nearly on the same orbit at altitude around 460 km with slight time difference, i.e., from 5 to 100 s for SWARM-A and SWARM-B, from 75 to 230 s for SWARM-B and SWARM-C, and from 30 to 100 s for SWARM-C and SWARM-A. Figure 1 shows the differences in time and in geographical location when the SWARM-A and SWARM-B pass the same geomagnetic (i.e., dipole) latitude. The time separation between SWARM-B and SWARM-C, and between SWARM-C and SWARM-A is also shown with red broken lines. The SWARM-B flew ahead of the SWARM-A about 5 s on 27 November and the difference almost linearly increased to 98 s until 21 January, and then started to decrease until 27 January. Because of the Earth's rotation, the longitudinal difference appears proportionally to the time separation although the maximum was about 0.4° (i.e., the maximum east-west separation is 40 km near the equator) on 21 January.

As the latitudinal scale of the field-aligned current circuit is typically 100–200 km [*Nakanishi et al.*, 2014], we assume that the longitudinal scale of the current system is also similar and we neglect the effect of the longitudinal difference in the following statistical analysis. The local time start from 14 LT on 27 November and decreases to 9 LT on 27 January. This local time variation could affect the signal-to-noise ratio through the ionospheric conductivity difference because the amplitude of magnetic fluctuations, i.e., the amplitude of signal, is much larger on the dayside than that on the nightside. However, we also neglect the effect because the conductivity difference is roughly within 20% on the dayside during the period.

The magnetic field data obtained by each SWARM satellite were high-pass filtered to subtract the Earth's main field, local (crustal) anomaly, and large-scale ionospheric and magnetospheric current effects by a B-spline fitting with the same method described in *Nakanishi et al.* [2014] for the CHAMP satellite data. The filtering cutoff period is around 40 s. We use the 1 s sampled data (resolution 0.065 nT) in sensor coordinate system approximately aligned to north-south (Z), east-west (Y), and vertical (X) without converting to the geographic coordinate system with the attitude data expecting very stable attitude as was the case of CHAMP satellite. The basic characteristics of the small-scale fluctuations thus obtained are essentially the same with that of the CHAMP satellite except for the statistical characteristics which have not yet been examined for the SWARM satellite data. That is, (1) they appear almost always, (2) they have rough magnetic

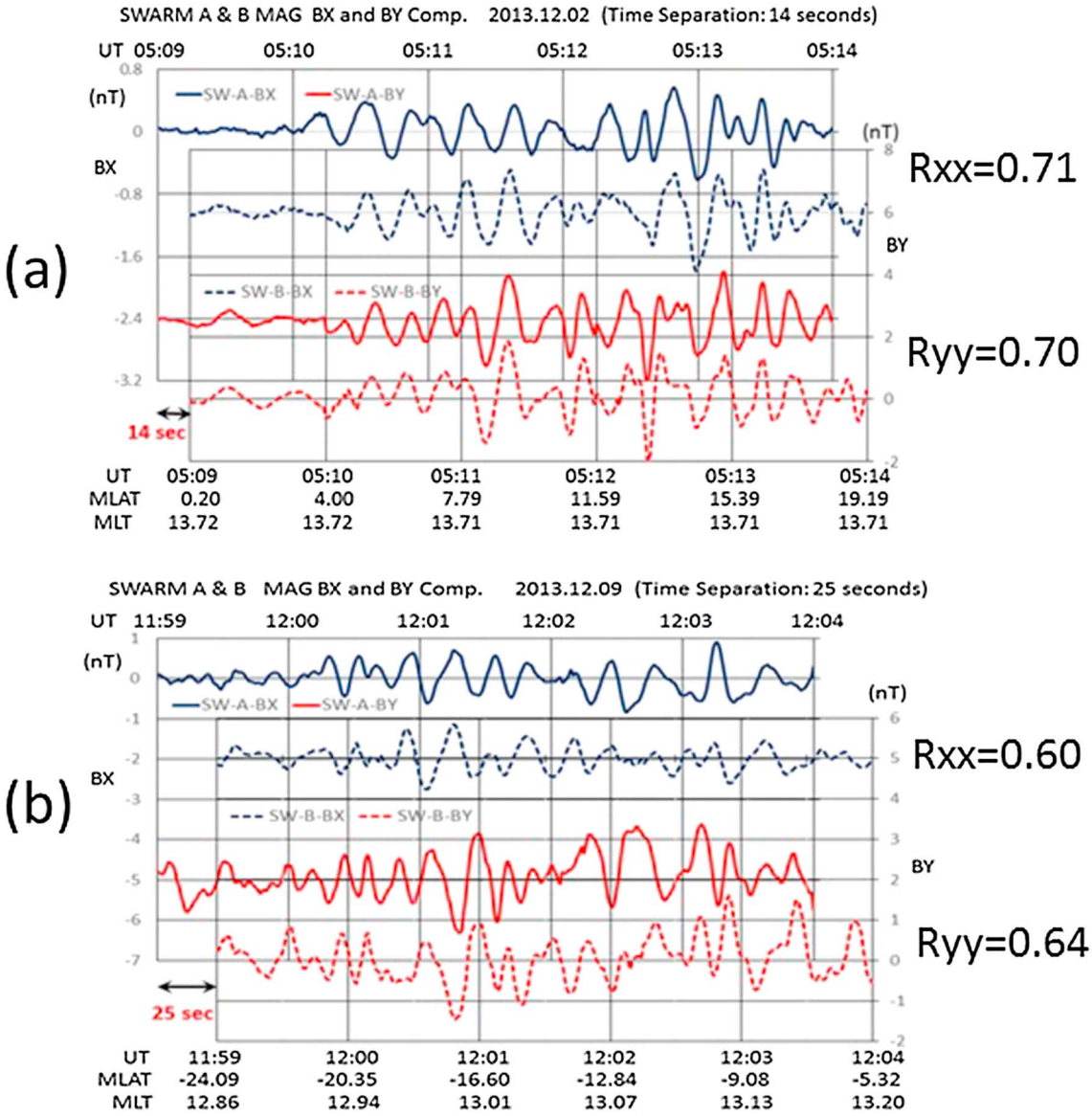

Figure 2. A comparison of the magnetic fluctuations (Blue; vertical component: Red; east-west component) observed by the SWARM-A and SWARM-B. The SWARM-B was 14 s ahead of the SWARM-A on (a) 2 December and 25 s on (b) 9 December 2013. The correlation coefficients for each component, *Rxx* (for *BX* of SWARM-A and SWARM-B) and *Ryy* (for *BY*), are shown.

conjugacy, (3) they are orthogonal to the geomagnetic main field, (4) the amplitude is much larger on the dayside, and (5) zonal component is larger than the meridional component in general.

Figures 2a and 2b show a comparison of the magnetic fluctuations (*BX*: vertical; *BY*: east-west component) observed by the SWARM-A and SWARM-B on 2 December and 9 December when the time difference, i.e., separation between the two satellites, was about 14 and 25 s, respectively. By shifting 14 and 25 s in each case, each two lines of same component from the two satellites show almost the same variation which clearly indicates that the magnetic fluctuations are the spatial structure along the satellite orbit rather than the temporal variation.

However, the difference of the fluctuations is slightly larger in the case on 9 December than that on 2 December as seen in Figure 2 by the correlation coefficient *Rxx* and *Ryy*, and this tendency of time separation dependence becomes clearer as the time separation increases. This difference can be the effect of the temporal variation of the field-aligned currents, and we may be able to estimate the time scale of the temporal variation using this tendency, which is essential to identify the source mechanism of the field-aligned currents.

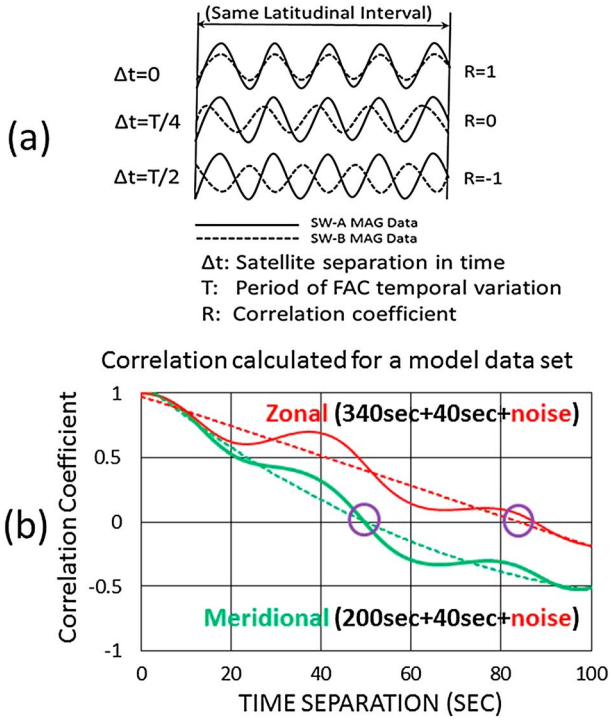

Figure 3. (a) A schematic drawing to show the relation between the phase shift between the observed data by the two satellites and their correlation coefficient. "*T*" is the period of the temporal variation at a fixed location, i.e., it is not the apparent period observed along the satellite orbit. (b) Variation of correlation coefficient for a given data set having temporal variation with periods of 40, 200, and 340 s with noise. The dashed lines are second-order polynomial fits to the correlation coefficients calculated from the modeled data set. (see text).

To estimate the scale of the temporal variation at fixed location in space, which we assume to be much slower than the time scale of satellite passing through a pair of field-aligned currents (i.e., 10–30 s), we use an in-flight method as described below. We firstly calculate the correlation coefficient between the data sets from two satellites for each interval of 120 s which covers the same latitudinal range by shifting the time difference determined from orbit information. They are calculated for the period when the two satellites are within ±50° geomagnetic latitude. The correlation coefficients are calculated with the data sets from three combinations of satellite pair, i.e., SWARM-A and SWARM-B, SWARM-B and SWARM-C, and SWARM-C and SWARM-A. Because of the initial schedule of SWARM orbit formation, more than half of the data set comes from a pair of SWARM-A and SWARM-B; however, we also use other pairs to fill the gap in time separation as much as possible. The range of time separation to be examined is limited within 100 s because the maximum separation of SWARM-A and SWARM-B pair during the period examined was 100 s as shown in Figure 1.

Because the amplitude is much different on the dayside and on the nightside due to the difference in the ionospheric conductivities as discussed by *Nakanishi et al.* [2014], we calculate correlation coefficients with the data obtained on the dayside (6–18 MLT) and with those on the nightside (18–06 MLT) separately. In this paper, we show in Figure 4 the results only on the dayside to avoid various effects from equatorial plasma bubbles on the nightside [e.g., *Lühr et al.*, 2014], the midlatitude electric field fluctuations, [see *Saito et al.*, 1995], and the nighttime midlatitude magnetic field fluctuations [see *Park et al.*, 2009]. To avoid contamination from artificial noise or some rapid events such as storm sudden commencements, we omit the interval which includes the fluctuation with amplitude greater than 10 nT.

The in-flight method for the estimate of time scale is as follow: As schematically depicted in Figure 3a as a very simple case, the correlation coefficient is zero when the phase difference is $T/4$ for two time series, here T is the period of the temporal variation at a fixed point on an orbit. That is, if we find the zero crossing of correlation coefficient at a time separation, τ, the period T is estimated to be 4τ in such simple case.

To check such estimate is possible or not when the field-aligned current varies with two or more different time scales, we calculated the correlation coefficients for a modeled data set (i.e., time series X and Y below). That is, they have the temporal variation with 40, 200, and 340 s and the "noise" which has the similar periods but independent phase assuming an injection of separate wave packet from different source to one of the two satellite orbits. Each data set has an interval of 120 s and it consists of five 24 s subintervals. For each subinterval, the modeled data are given with the following equations:

$$X(t) = a\,\sin(\omega_1 t + \varphi_1) + b\,\sin(\omega_2 t + \varphi_2)$$
$$Y(t) = a\,\sin(\omega_1 t + \varphi_1 + \Omega_1 \delta T) + b\,\sin(\omega_2 t + \varphi_2 + \Omega_2 \delta T) + N(t)\delta T/100$$
$$N(t) = c\,\sin(\omega_1 t + \varphi_3 + \Omega_1 \delta T) + d\,\sin(\omega_2 t + \varphi_4 + \Omega_2 \delta T)$$

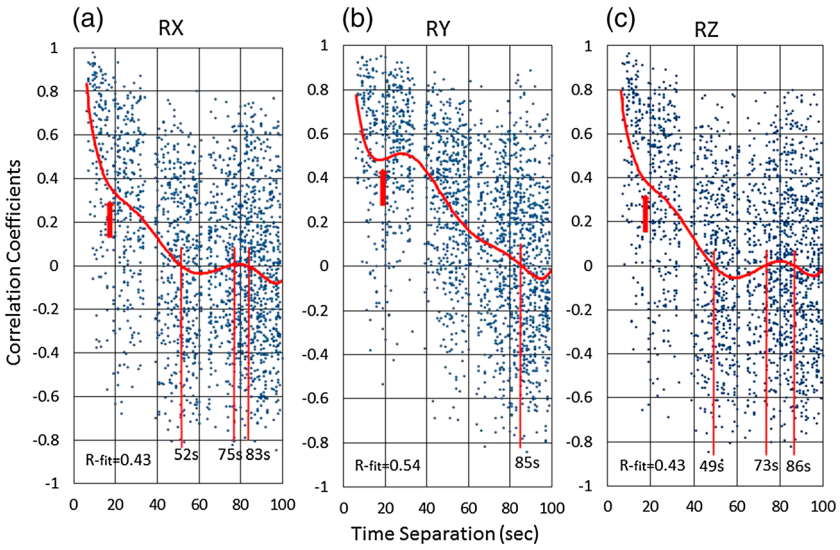

Figure 4. A dependence of correlation coefficients on the time separation between all pairs of the SWARM-A, SWARM-B, and SWARM-C. (a) *RX*, (b) *RY*, and (c) *RZ* are for vertical, east-west, and north-south components in the sensor coordinate system, respectively. The vertical red lines indicate the zero-crossing points of the polynomial fitted lines of the correlation coefficients. "R fit" indicates the correlation coefficient between the correlation dots and their six-order polynomial fit.

$X(t)$, $Y(t)$, $N(t)$: Modeled time series for satellite A, B, and noise (i.e., independent wave packet having amplitude which increases proportional with time separation), respectively. Here
ω_1, ω_2: apparent frequency along the orbit (period = 30 and 20 s, respectively)
Ω_1, Ω_2: Frequency of "temporal" variation (Ω_1: period = 200 and 340 s for meridional component and for zonal component, respectively; Ω_2: 40 s for both components)
δT: Time separation (0 ~ 200 s).

The time series *X* and *Y* are generated for five intervals (i.e., 24 s × 5 sets), and "*a*," "*b*," "*c*," "*d*," and "φ" are different (at random) for each 24 s interval. For example, in a 120 s interval used in Figure 3b, in the first 24 s interval, (a, b, c, d, φ_1, φ_2, φ_3, φ_4) = (0.5, 0.45, 1.5, 0.25, 2.62, 0.52, 0.52, and 2.62) and in other four intervals, the parameters are given at random with similar magnitude, and coefficients *b* and *c* are smaller (i.e., half or less) than *a* and *c* on average assuming that the amplitude of shorter period (40 s) is smaller than that of longer one (200 or 340 s). The sign of ω_1 and ω_2 is also changed at random. Although the parameters in the above equations can be arbitrary as a modeled data set, we use the period of temporal variation estimated from real data, i.e., the period estimated from Figure 4 (i.e., 40, 200, and 340 s).

Figure 3b shows the variation of the modeled correlation coefficient with time separation thus calculated. The dotted lines are second-order polynomial fit to identify the zero crossing by eliminating the effect from short-period variation. Although the modeled time series are much complicated than that in Figure 3a, the zero-crossing points roughly correspond to the quarter of given period of temporal variation (i.e., 200 and 340 s) and we also see the dip around 20 s which corresponds to the half of 40 s variation. That is, the given periods are approximately reproduced as the zero-crossing points and a dip of correlation coefficient. Because the modeled time series used in Figure 3b is still too simple and hence the correspondence shown in Figure 3b does not validate in logical sense our estimate from real data as shown in the next section, it supports that our method roughly works even in the case having multiperiod variations and "noise" component if it is not very complicated.

3. Results

Figure 2 clearly shows that the magnetic fluctuations around 10–30 s are spatial structure of field-aligned currents along the satellite orbit having latitudinal scale about 70–210 km because the fluctuations observed by two satellites show almost identical variation by shifting the time axis by the time separation. This clearly

confirms the existence of small spatial scale field-aligned currents expected from several indirect evidences obtained by the CHAMP data analysis [*Nakanishi et al*., 2014].

Figure 4 shows the dependence of correlation coefficients on the time separation between two satellites. The number of the data sets, each covers 120 s interval in middle or low latitudes on the dayside, is 2001. Adjacent 120 s intervals have no overlapping. Each dot in the panels labeled RX, RY, and RZ indicates the correlation coefficient of the vertical, east-west, and north-south components, respectively. The red curves are 6 order polynomial fit to the correlation dots. The fitting efficiency, *R* fit, is indicated by a correlation coefficient between the polynomial curve and correlation dots in each panel. The vertical red lines indicate the location where the polynomial fits cross the zero line of the correlation coefficient.

During the period shortly after the launch of the satellites, the correlation coefficients are rather high, i.e., around 0.7–0.8 on average for all three components, and they gradually decreases as the separation between the satellites increases with time. This decrease may be attributed to the temporal variation of the field-aligned current intensity and direction which modifies the phase of the magnetic fluctuations at fixed latitude. If this is the case, we can estimate the typical time scale of the current variation by the method explained in previous section.

In the actual case, the situation is much more complicated and, in fact, there exist considerable scatter of the correlation coefficients. One possible cause of the scatter is the case when no current (or very weak one) exists in 120 s interval. In such case the correlation coefficient is low in general or could be high or negative by chance. Another possibility is when an effect from crustal anomaly is not removed by the filtering process. In such case, the correlation coefficient could be high. Some magnetospheric processes including micropulsations could also be a cause. In spite of the large scatter of the coefficients, one remarkable point is that the polynomial fits to *BX* and *BZ* are almost identical though the two components are observed independently from separate sensor axis. This may indicate to some extent the reliability of the smoothed curve.

Figure 4 shows that the smoothed value, i.e., the polynomial fitted value becomes zero around 50, 74, and 85 s of time separation for the vertical (*BX*) and north-south (*BZ*) components (i.e., meridional) and around 85 s for east-west (*BY*) component (i.e., zonal). Although the calculation of correlation coefficient is nonlinear manipulation and we need to be careful to interpret the results, these results, i.e., zero-crossing points suggest that the typical time scale of the field-aligned current variation is roughly about 200 (= 50×4), 296 (= 74×4), and 340 (= 85×4) s for the current which produces the meridional component and around 340 s for the currents which produce the zonal component.

A clear dip is seen at around 15–25 s of time separation. If this dip is produced by a component having shorter-period temporal variation with antiphase, then the period is estimated to be 30–50 s.

4. Discussion and Conclusion

In the paper by *Nakanishi et al*. [2014], it was suggested that the ionospheric dynamo is caused by the neutral atmospheric waves such as the acoustic gravity waves or internal gravity waves generated by the lower atmospheric disturbances. On the ground, in particular after big earthquakes, the vertical acoustic resonance frequency such as the periods around 200, 230, and 270 s is often observed in both magnetic field and microbarometric data [*Iyemori et al*., 2005, 2013]. *Zettergren and Snively* [2013] showed by a numerical simulation that the field-aligned currents are generated by acoustic mode waves. Taking into account these previous results, it is plausible that the neutral atmospheric waves generated by the lower atmospheric disturbances are the source of the small-scale field-aligned currents.

The estimated time scales, i.e., 200, 296, and 340 s, are within the period of acoustic mode waves near the cutoff in the ionosphere. One remarkable point is that the periods 200 and 296 s are close to two of the theoretically predicted three major periods of the vertical acoustic resonance [e.g., see *Shinagawa et al*., 2007, and references therein]. The longer period, 340 s, is close to the cutoff period at 130 km altitude where the ionospheric dynamo can occur and it is still in the period range of acoustic mode. Although the significance of the second (296 s) and third (340 s) zero crossings in meridional component is not clear at the stage of this initial analysis, these results indicate that the main cause of the field-aligned currents is the acoustic mode gravity waves.

The scatter of the correlation coefficient may also come from the contamination of more short time scale phenomena. For example, the dip of the correlation coefficient around 15–25 s time separation in Figure 4 might reflect the effect of the waves with shorter time scale around 30–50 s, i.e., antiphase effect at *T*/2 in Figure 4a. The effect of longitudinal separation (maximum 0.4°) caused by the Earth's rotation as seen in Figure 1 seems to be negligible because of the very small latitudinal dependence of the correlation coefficient (not shown in this paper).

The difference of the estimated time scale for the meridional component (200 s and possibly 296 and 340 s) and for the zonal component (340 s), i.e., the existence of shorter time scale (200 s) in meridional component, could indicate the existence of independent current circuits (i.e., closure) having different altitude of the source dynamo region in the ionosphere. That is, the possible difference in the current circuit may reflect the difference of the cutoff period of the acoustic waves where the ionospheric dynamo takes place. The three-dimensional analysis of the field-aligned current circuit and investigation of energy flow direction along the geomagnetic field lines may be the next step of this research with the SWARM satellite data to confirm the suggestions from this initial report.

Acknowledgments
This study is a part of the research proposal (ID: 10230) to the Swarm Science and Validation Opportunity Project under the ESA. The data used in this paper are available from ESA's FTP server at the IP address 131.176.196.17 with detailed explanation at https://earth.esa.int/web/guest/missions/esa-operational-eo-missions/swarm. This study was supported by grant 25287128 under Japan Society for Promotion of Science (JSPS). We thank M. Nose for his valuable discussion.

The Editor thanks Arthur Richmond and an anonymous reviewer for their assistance in evaluating this paper.

References

Heilig, B., H. Lühr, and M. Rother (2007), Comprehensive study of ULF upstream waves observed in the topside ionosphere by CHAMP and on the ground, *Ann. Geophys.*, *25*, 737–754.

Iyemori, T., et al. (2005), Geomagnetic pulsations caused by the Sumatra earthquake on December 26, 2004, *Geophys. Res. Lett.*, *32*, L20807, doi:10.1029/2005GL024083.

Iyemori, T., et al. (2013), Barometric and magnetic observations of vertical acoustic resonance and resultant generation of field-aligned current associated with earthquakes, *Earth Planets Space*, *65*, 901–909.

Lühr, H., C. Xiong, J. Park, and J. Rauberg (2014), Systematic study of intermediate-scale structures of equatorial plasma irregularities in the ionosphere based on CHAMP observations, *Front. Phys.*, doi:10.3389/fphy.2014.00015.

Nakanishi, K., T. Iyemori1, K. Taira, and H. Lühr (2014), Global and frequent appearance of small spatial scale field aligned currents possibly driven by the lower atmospheric phenomena as observed by the CHAMP satellite in middle and low latitudes, *Earth Planets Space*, *66*, 40, doi:10.1186/1880-5981-66-4.

Park, J., H. Lühr, C. Stolle, M. Rother, K. W. Min, J.-K. Chung, Y. H. Kim, I. Michaelis, and M. Noja (2009), Magnetic signatures of medium-scale traveling ionospheric disturbances as observed by CHAMP, *J. Geophys. Res.*, *114*, A03307, doi:10.1029/2008JA013792.

Saito, A., T. Iyemori, M. Sugiura, N. C. Maynard, T. L. Aggson, L. H. Brace, M. Takeda, and M. Yamamoto (1995), Conjugate occurrence of the electric fluctuations in the nighttime midlatitude ionosphere, *J. Geophys. Res.*, *100*, 21,439–21,451, doi:10.1029/95JA01505.

Shinagawa, H., T. Iyemori, S. Saito, and T. Maruyama (2007), A numerical simulation of ionospheric and atmospheric variations associated with the Sumatora earthquake on December 26, 2004, *Earth Planets Space*, *59*, 1015–1026.

Zettergren, M. D., and J. B. Snively (2013), Ionospheric signatures of acoustic waves generated by transient tropospheric forcing, *J. Geophys. Res. Lett.*, *40*, 5345–5349, doi:10.1002/2013GL058018.

Erratum

In the original version of this article, several instances of the direction of sensor axes appeared incorrectly in Sections 2 and 3, and in the legends of Figures 2 and 4. These errors have been corrected, and this version may be considered the authoritative version of record.

In section 2, paragraph 3, "north-south (*X*)" has been corrected to "north-south (*Z*)", and "vertical (*Z*)" has been corrected to "vertical (*X*)".

In section 2, paragraph 4, "north-south" has been corrected to "vertical".

In section 3, paragraph 2, "north-south, east-west, and vertical" has been corrected to "vertical, east-west, and north-south".

In section 3, paragraph 5, "north-south" has been corrected to "vertical", and "vertical" has been corrected to "north-south".

In the legend of Figure 2, "north-south" has been corrected to "vertical"; and in the legend of Figure 4, "north-south, east-west, and vertical" has been corrected to "vertical, east-west, and north-south".